METEOROLOGICAL RADAR

The origins of meteorological radar (RAdio Detection And Ranging) can be traced to the 1920s when the first echoes from the ionosphere were observed with dekametric (tens of meters) wavelength radars. However, the greatest advances in radar technology were driven by the military's need to detect aircraft and occurred in the years leading to and during WWII. (A brief review of the earliest meteorological radar development is given in Ref. 1; a detailed review of the development during and after WWII is given in Ref. 2.) Precipitation echoes were observed almost immediately with the deployment of the first decimeter (≈0.1 m) wavelength military radars in the early 1940s. Thus, the earliest meteorological radars used to observe weather (i.e., weather radars) were manufactured for military purposes. The military radar's primary mission is to detect, resolve, and track discrete targets such as airplanes coming from a particular direction, and to direct weapons for interception.

Although weather radars also detect aircraft, their primary objective is to map the intensity of precipitation (e.g., rain, or hail), which can be distributed over the entire hemisphere above the radar. Each hydrometeor's echo is very weak; nevertheless, the extremely large number of hydrometeors within the radar's beam returns a continuum of strong echoes as the transmitted pulse propagates through the field of precipitation. Thus, the weather radar's objective is to estimate and map the fields of reflectivity and radial velocities of hydrometeors; from these two fields the meteorologists need to derive the fall rate and accumulation of precipitation and warnings of storm hazards. The weather radar owes its success to the fact that centimetric waves penetrate extensive regions of precipitation (e.g., hurricanes) and reveal, like an X-ray photograph, the morphology of weather system.

The first U.S. national network of weather radars, designed to map the reflectivity fields of storms and to track them, were built in the mid 1950s and operated at 10 cm wavelengths. 1988 marked the deployment of the first network of Doppler weather radars (i.e., the WSR-88D), which in addition to mapping reflectivity, have the capability to map radial (Doppler) velocity fields. This latter capability proved to be very helpful in identifying those severe storm cells that harbor tornadoes and damaging winds.

If a hydrometeor's diameter is smaller than a tenth of the radar's wavelength, its echo strength is inversely proportional to the fourth power of the wavelength. Thus, shorter wavelength (i.e., millimeter) radars are usually the choice to detect clouds. Cloud particle diameters are less than 100 μ, and attenuation due to cloud particles is not overwhelming. However, if clouds bear rain of moderate intensity, precipitation attenuation can be severe (e.g., at a wavelength of 6.2 mm, and rainrate of 10 mm h^{-1}, attenuation can be as much as 6 dB km^{-1} (3). Spaceborne meteorological radars also operate in the millimetric band of wavelengths in order to obtain acceptable angular resolution with reasonable antenna diameters required to resolve clouds at long ranges (4). Airborne weather radars operate at short wavelengths of approximately 3 and 5 cm; these are used to avoid severe storms that produce hazardous wind shear and extreme amounts of rainwater (which extinguish jet engines), and to study weather phenomena (5). The short wavelength waves are used to obtain acceptable angular resolution with small antennas on aircraft; however, short waves are strongly attenuated as they propagate into heavy precipitation. At longer wavelengths (e.g., >10 cm), only hail and heavy rain significantly attenuate the radiation.

Weather radars are commonly associated with the mapping of precipitation intensity. Nevertheless, the earliest, of what we now call, meteorological radars detected echoes from the nonprecipitating troposphere in the late 1930s (1,2). Scientists determined that these echoes are reflected from the dielectric boundaries of different air masses (1,6). The refractive index n of air is a function of temperature and humidity, and spatial irregularities in these parameters, caused by turbulence, were found to be sufficiently strong to cause detectable echoes from refractive index irregularities.

FUNDAMENTALS OF METEOROLOGICAL DOPPLER RADAR

The basic principles for meteorological radars are the same as for any radar that transmits a periodic train of short duration pulses (i.e., with period T_s called the pulse repetition time (PRT), and duration τ) of microwaves, and measures the delay between the time of emission of the transmitted pulse and the time of reception of any of its echoes. The PRT (i.e., T_s) is typically of the order of milliseconds, and pulsewidths τ are of the order of microseconds. The radar has Doppler capability if it can measure the change in frequency or wavelength between the backscattered and transmitted signals.

The Doppler radar's microwave oscillator (Fig. 1) generates a continuous wave sinusoidal signal, which is converted to a sequence of microwave pulses by the pulse modulator. Therefore, the sinusoids in each microwave pulse are coherent with those generated by the microwave oscillator; that is, the crests and valleys of the waves in the pulse bear a fixed or known relation between the crests and valleys of the waves emitted by the microwave oscillator. The microwave pulses are then amplified by a high-power amplifier (a klystron is used in the WSR-88D) to produce about a megawatt of peak power. The propagating pulse has a spatial extent of $c\tau$, and travels at the speed of light c along the beam (beamwidth θ_1 is the one-way, 3 dB width of the beam, and is of the order of 1 degree). The transmit/receive (T/R) switch connects the transmitter to the antenna (an 8.53 m diameter parabolic reflector is used for the WSR-88D) during τ, and the receiver to the antenna during the interval $T_s - \tau$. The echoes are mixed in the synchronous detectors with a pair of phase quadrature signals (i.e., sine, 90°, and cosine, 0°, outputs from the oscillator). The pair of synchronous detectors and filter amplifiers shift the carrier frequency from the microwave band to zero frequency in one step for the homodyne radar and allow measurement of both positive and negative Doppler shifts (most practical radars use a two step process involving an intermediate frequency).

A hydrometeor intercepts the transmitted pulse and scatters a portion of its energy back to the antenna, and the echo voltage

$$V(r,t) = Ae^{j[2\pi f(t-2r/c)+\psi)}U(t-2r/c) \tag{1}$$

at the input to the synchronous detectors is a replica of the signal transmitted; A is the echo amplitude that depends on the hydrometeor's range r and its backscattering cross section σ_b, and $2\pi f(t - 2r/c) + \psi$ is the echo phase. The microwave carrier frequency is f, t is time after emission of the transmitted pulse, and ψ is the sum of phase shifts introduced by the radar system and by the scatterer; these shifts are usually independent of time. The function U locates the echo; it is one when its argument is between zero and τ, and zero otherwise. The output of one synchronous detector is called the in-phase (I) voltage and the other is called the quadrature-phase (Q) voltage (Fig. 1); these are the imaginary and real parts of the echo's complex voltage [Eq. (1)] after its carrier frequency f is shifted to zero. Thus

$$I(t,r) = A\cos\psi_e U(t-2r/c), \quad Q(r,t) = A\sin\psi_e U(t-2r/c) \tag{2}$$

where

$$\psi_e = -\frac{4\pi r}{\lambda} + \psi \tag{3}$$

is the echo phase, and $\lambda = c/f$ is the wavelength of the transmitted microwave pulse. The time rate of the echo phase change is related to the scatterer's radial (Doppler) velocity ν,

$$\frac{d\psi_e}{dt} = -\frac{4\pi}{\lambda}\frac{dr}{dt} = -\frac{4\pi}{\lambda}\nu = \omega_d \tag{4}$$

where ω_d is the Doppler shift (in radians per second). For typical transmitted pulse widths (i.e., $\tau \approx 10^{-6}$ s) and hydrometeor velocities (tens of m s^{-1}), the changes in phase are extremely small during the time that $U(t - 2r/c)$ is nonzero. Therefore, the echo phase change is measured over the longer PRT period ($T_s \approx 10^{-3}$ s) and, consequently, the pulse Doppler weather radar is both an amplitude– and phase–sampling system. Samples are at $\tau_s + mT_s$, where τ_s is the time delay between a transmitted pulse and an echo, and m is an integer; τ_s is a continuous time scale and always lies in the interval $0 \le \tau_s \le T_s$, and mT_s is called sample time, which increments in T_s steps.

Because the transmissions are periodic, echoes repeat, and thus, there is no way to determine which transmitted pulse produced which echo (Fig. 2). That is, because τ_s is measured with respect to the most recent transmitted pulse and has values $< T_s$, the apparent range $c\tau_s/2$ is always less than the unambiguous range $r_a = cT_s/2$. However, the true range r can be $c\tau_s/2 + (N_t - 1)r_a$, where N_t is the trip number, and $N_t - 1$ designates the number of $cT_s/2$ intervals that need to be

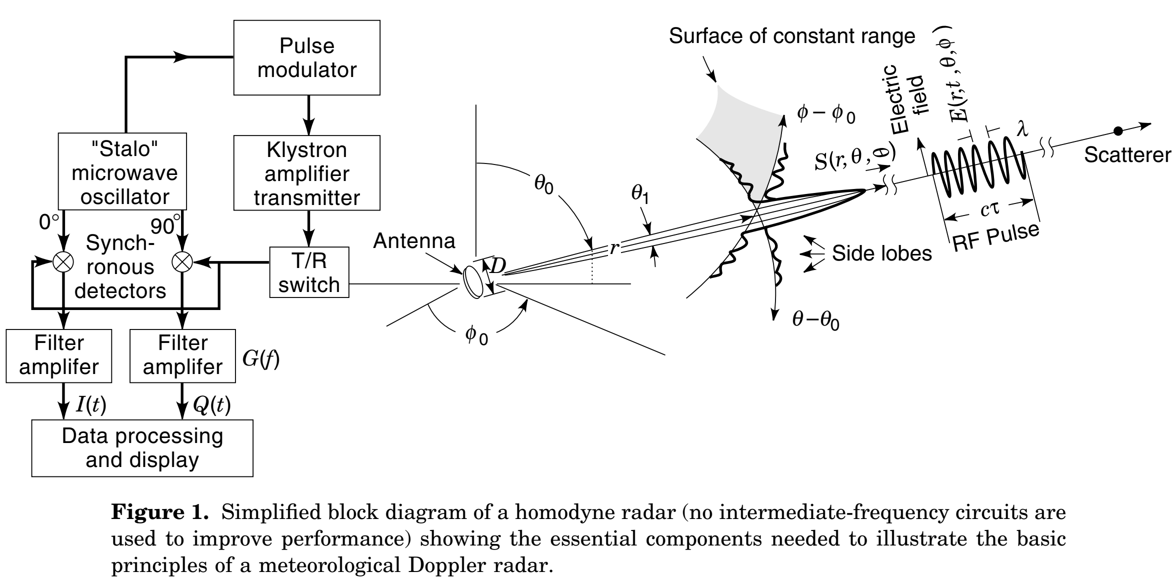

Figure 1. Simplified block diagram of a homodyne radar (no intermediate-frequency circuits are used to improve performance) showing the essential components needed to illustrate the basic principles of a meteorological Doppler radar.

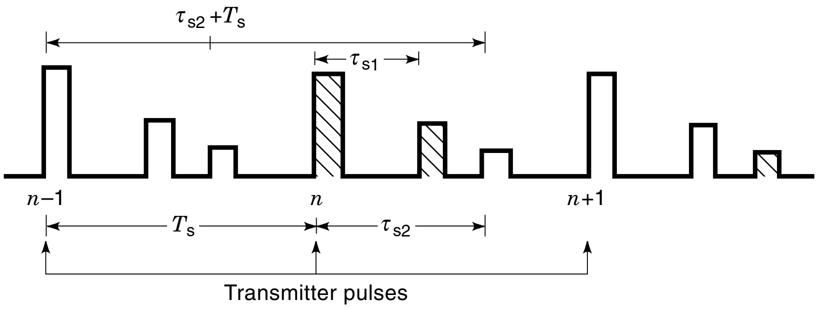

Figure 2. Range-ambiguous echoes. The nth transmitted pulse and its echoes are crosshatched. This example assumes that the larger echo at delay τ_{s1} is unambiguous in range, but the smaller echo, at delay τ_{s2}, is ambiguous. This smaller second trip echo, which has a true range time delay $T_s + \tau_{s2}$, is due to the $(n - 1)$th transmitted pulse.

added to the apparent range to obtain r. There is range ambiguity if $r \geq r_a$.

The I and Q components of echoes from stationary and moving scatterers are shown in Fig. 3 for three successive transmitted pulses. The echoes from the moving scatterer clearly exhibit a systematic change, from one $m\mathrm{T}_s$ period to the next, caused by the scatterers' Doppler velocity, whereas there is no change in echoes from stationary scatterers. Echo phase $\psi_e = \tan^{-1}(Q/I)$ is measured, and its change over T_s is proportional to the Doppler shift given by Eq. (4).

The periodic transmitted pulse sequence also introduces velocity ambiguities. A set of ψ_e samples cannot be related to one unique Doppler frequency. As Fig. 4 shows, it is not possible to determine whether $V(t)$ rotated clockwise or counterclockwise and how many times it circled the origin during the interval T_s. Therefore, any of the frequencies $\Delta\psi_e/\mathrm{T}_s + 2\pi p/T_s$ (where p is a $\pm$ integer, and $-\pi < \Delta\psi_e \leq \pi$) could be correct. All such Doppler frequencies are called aliases, and $f_N = \omega_N/2\pi = 1/(2T_s)$ is the Nyquist frequency (in units of Hertz). All Doppler frequencies between $\pm f_N$ are the principal aliases, and frequencies higher or lower than $\pm f_N$ are ambiguous with those between $\pm f_N$. Thus, hydrometeor radial velocities must lie within the unambiguous velocity limits, $\nu_a = \pm\lambda/4T_s$, to avoid ambiguity. Signal design and processing methods have been advanced to deal with range-velocity ambiguities (1).

REFLECTIVITY AND VELOCITY FIELDS OF PRECIPITATION

A weather signal is a composite of echoes from a continuous distribution of hydrometeors. After a delay (the roundtrip time of propagation between the radar and the near boundary of the volume of precipitation), echoes are continuously received (Fig. 5) during a time interval equal to twice the time it takes the microwave pulse to propagate across the volume containing the hydrometeors. Because one cannot resolve each of the hydrometeor's echoes, meteorological radar circuits sample the I and Q signals at uniformly spaced intervals along τ_s, and convert the analog values of the I, Q voltages to digital numbers. For each sample, there is a resolution volume V_6 (i.e., the volume enclosed by the surface on which angular and range-weighting functions (1) are smaller than 6 dB below their peak value) along the beam within which hydrometeors contribute significantly to the sample. Each scatterer within V_6 returns an echo and, depending on its precise position to within a wavelength, its corresponding I or Q can have any value between maximum positive and negative excursions. Echoes from the myriad of hydrometeors constructively or destructively (depending on their phases) interfere with each other to produce the composite weather signal voltage $V(mT_s, \tau_s) = I(mT_s, \tau_s) + jQ(mT_s, \tau_s)$ for the mth T_s interval. The random size and location of hydrometeors cause the I and Q weather signals to be a random function of τ_s. How-

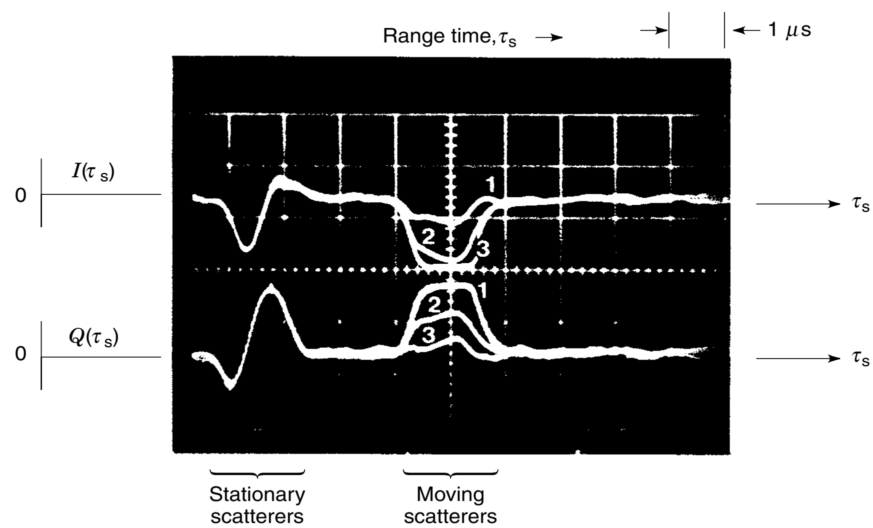

Figure 3. $I(\tau_s)$ and $Q(\tau_s)$ signal traces vs τ_s for three successive sampling intervals T_s have been superimposed to show the relative change of I, Q for both stationary and moving scatterers.

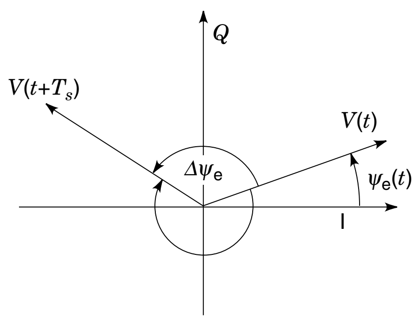

Figure 4. A phasor diagram used to depict frequency aliasing. The phase of the signal sample $V(t)$ could have changed by $\Delta\psi_e$ over a period T_s.

ever, these random signals have a correlation time τ_c (Fig. 5), dependent on the pulsewidth τ and the receiver's bandwidth (1). Thus, $V(mT_s, \tau_s$ has noise-like fluctuations along τ_s even if the scatterer's time averaged density is spatially uniform.

The sequences of $M(m = 1 \rightarrow M)$ samples at any τ_s are analyzed to determine the motion and reflectivity of hydrometeors in the corresponding V_6. The dashed line in Fig. 5 depicts a possible sample time mT_s, dependence of $I(mT\text{s}, \tau_{s1})$ for hydrometeors having a mean motion that produces a slowly changing sample amplitude along mT_s. The rate of change of I and Q vs mT_s is determined by the radial motion of the scatterers. Because of turbulence, scatterers also move relative to one another and, therefore, the I, Q samples at any τ_s change randomly with a correlation time along mT_s dependent on the relative motion of the scatterers. For example, if turbulence displaces the relative position of scatterers a significant fraction of a wavelength during the T_s interval, the weather signal at τ_s will be uncorrelated from sample to sample, and Doppler velocity measurements will not be possible; Doppler measurements require a relatively short T_s.

The random fluctuations in the I, Q samples have a Gaussian probability distribution with zero mean; the probability of the signal power $I^2 + Q^2$ is exponentially distributed (e.g., the weakest power is most likely to occur). Using an analysis of the $V(mT_s, \tau_s)$ sample sequence along mT_s, the meteorological radar's signal processor to estimate both the average sample power and the power-weighted velocity of the scatterers accurately. The samples' average power $\overline{P}$ is

$$\overline{P}(r_o) = \iiint \eta(\boldsymbol{r}) I(\boldsymbol{r}_o, \boldsymbol{r})\, dV \tag{5}$$

in which the reflectivity η, the sum of the hydrometeor backscattering cross sections σ_b per unit volume, is

$$\eta(\boldsymbol{r}) = \int_0^\infty \sigma_b(D) N(D, \boldsymbol{r})\, dD \tag{6}$$

The factor $I(\boldsymbol{r}_o, \boldsymbol{r})$ in Eq. (5) is a composite angular and range-weighting function; its center at $\boldsymbol{r}_o$ depends on the beam direction as well as τ_s. The values of $I(\boldsymbol{r}_o, \boldsymbol{r})$ at $\boldsymbol{r}$ depend on the antenna pattern, transmitted pulse shape and width, and the receiver's frequency or impulse transfer function (1). In general, $I(\boldsymbol{r}_o, \boldsymbol{r})$ has significant values only within V_6; $N(D)$, the particle size distribution, determines the expected number density of hydrometeors with equivolume diameters between D and $D + dD$.

The meteorological radar equation,

$$\overline{P}(r_o) = \frac{P_t g^2 g_s \lambda^2 \eta c \tau \pi \theta_1}{(4\pi)^3 r_o^2 l^2 l_r 16 \ln 2} \tag{7}$$

is used to determine η from measurements of $\overline{P}$, wherein P_t is the peak transmitted power, g is the gain of the antenna (a larger antenna directs more power density along the beam and hence has larger gain), and g_s is the gain of the receiver (e.g., the net sum of losses and gains in the T/R switch, the synchronous detectors, and the filter/amplifiers in Fig. 1). Here $r_o \approx c\tau_s/2$, l is one-way atmospheric transmission loss, and l_r is the loss due to the receiver's finite bandwidth (1). Equation (7) is valid for transmitted radiation having a Gaussian function dependence on distance from the beam axis, and for uniform reflectivity fields.

Radar meteorologists have related reflectivity η, which is general radar terminology for the backscattering cross section per unit volume, to a reflectivity factor Z which has meteorological significance. If hydrometeors are spherical and have diameters much smaller than λ (i.e., the Rayleigh approximation), the reflectivity factor,

$$Z = \int_0^\infty N(D, \boldsymbol{r}) D^6\, dD \tag{8}$$

is related to η by

$$\eta = \frac{\pi^5}{\lambda^4} |K_m|^2 Z \tag{9}$$

where $K_m = (m^2 - 1)/(m^2 + 2)$, and $m = n(1 - j\kappa)$ is the hydrometeor's complex refractive index, and κ is the attenuation index (1).

The relation between radial velocity $\nu(\boldsymbol{r})$ at a point $\boldsymbol{r}$ and the power–weighted Doppler velocity $\overline{\nu}(\boldsymbol{r}_o)$ is

$$\overline{\nu}(\boldsymbol{r}_o) \frac{\iiint \nu(\boldsymbol{r}) \eta(\boldsymbol{r}) I(\boldsymbol{r}_o, \boldsymbol{r})\, dV}{\overline{P}(\boldsymbol{r}_o)} \tag{10}$$

It can be shown (1) that $\overline{\nu}(\boldsymbol{r}_o)$ is the first moment of the Doppler spectrum. An example of a Doppler spectrum for echoes

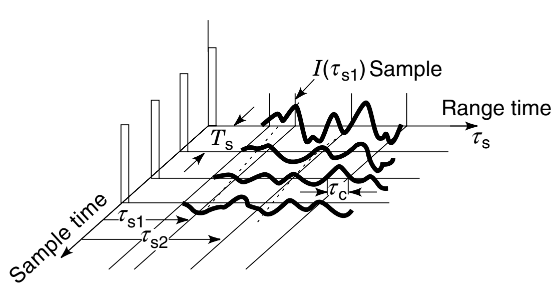

Figure 5. Idealized traces for $I(\tau_s)$ of weather signals from a dense distribution of scatterers. A trace represents $V(mT_s, \tau_s)$ vs τ_s for the mth T_s interval. Instantaneous samples are taken at sample times τ_{s1}, τ_{s2}, etc. The signal correlation time along τ_s is τ_c. Samples at fixed τ_s are acquired at T_s intervals and are used to compute the Doppler spectrum for scatterers located about the range $c\tau_s/2$.

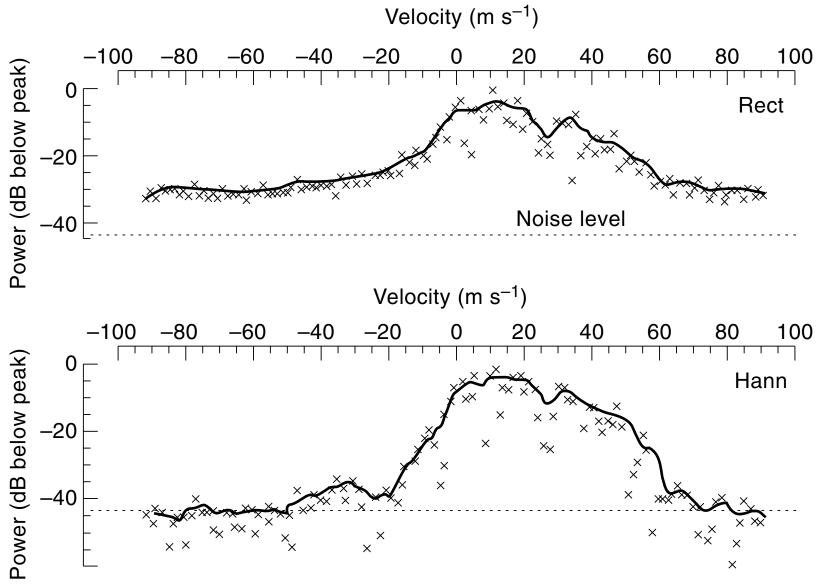

Figure 6. The spectral estimates (denoted by ×) of the Doppler spectrum of a small tornado that touched down on 20 May 1977 in Del City, Oklahoma. V_6 is located at azimuth: 6.1°; elevation: 3.1°; altitude: 1.9 km. Rect signifies the spectrum for weather signal samples weighted by a rectangular window function (i.e., uniform weight), whereas Hann signifies samples weighted by a von Hann window function (1).

from a tornado is plotted in Fig. 6. This power spectrum is the magnitude squared of the spectral coefficients obtained from the discrete Fourier transform for M = 128 $V(mT_s, \tau_s)$ samples at a τ_s corresponding to a range of 35 km. The obscuration of the maximum velocity (i.e., ≈60 m s^{-1}) of the scatterers in this tornado, and the power of stronger spectral coefficients leaked through the spectral sidelobes of the rectangular window (i.e., uniform weighting function) are evident. The von Hann weighting function reduces this leakage and better defines both true signal spectrum and maximum velocity. Where spectral leakage is not significant (e.g., samples weighted with the von Hann window function), the spectral coefficients have an exponential probability distribution and hence there is a large scatter in their power. Thus, a 5-point running average is plotted to show the spectrum more clearly. The spectral density of the receiver's noise is also obscured by the leakage of power from the larger spectral components if voltage samples are uniformly weighted.

RAIN, WIND, AND OBSERVATIONS OF SEVERE WEATHER

Fields of reflectivity factor Z and the power-weighted mean velocities $\bar{v}(\boldsymbol{r}_o)$ are displayed on color TV monitors to depict the morphology of storms. The Z at low elevation angles is used to estimate rain rates because hydrometeors there are usually rain drops, and vertical air motion can be ignored so that the drops are falling at their terminal velocity w_t, a known function of D. The rainfall rate R is usually measured as depth of water per unit time and is given by

$$R = \frac{\pi}{6}\int_0^\infty D^3 N(D)\omega_t(D)\,dD\,ms^{-1} \tag{11}$$

where mks units are used. To convert to the more commonly used units of millimeters per hour, multiply Eq. (11) by the factor 3.6 × 10^6. The simple and often observed $N(D)$ is an exponential one, and even in this case, we need to measure or specify two parameters of $N(D)$ to use Eq. (11). A real drop-size distribution requires an indefinite number of parameters to characterize it and thus, the radar-determined value of Z alone cannot provide a unique measurement of R. Although radar meteorologists have attempted for many years to find a useful formula that relates R to Z, there is unfortunately no universal relation connecting these parameters. Nonetheless, it is common experience that larger rainfall rates are associated with larger Z. For stratiform rain, the relation

$$Z = 200R^{1.6} \tag{12}$$

has often proved quite useful.

Although the Doppler radar measures only the hydrometeor motion toward and away from the radar, the spatial distribution of Doppler velocities can reveal meteorological features such as tornadoes, microbursts (i.e., the divergent flow of strong thunderstorm outflow near the ground), buoyancy waves, etc. For example, the observed Doppler velocity pattern for a tornado in a mesocyclone (a larger-scale rotating air mass) is shown in Fig. 7. The strong gradient of Doppler velocities associated with a couplet of closed ± isodops (i.e., contours of constant Doppler velocity) is due to the tornado having a diameter of about 700 m, and the larger-scale closed isodop pattern (i.e., the −30 and +20 contour) is due to the larger scale (i.e., 3.8 km diameter) mesocyclone. In practice, the data are shown on color TV displays wherein the regions between ± isodops are often colored with red and green hues of varying brightness to signify values of $\pm\bar{v}(\boldsymbol{r}_o)$.

A front is a relatively narrow zone of strong temperature gradients separating air masses. A dry line is simply the boundary between dry and moist air masses. Turbulent mixing along these boundaries creates relatively intense irregularities of refractive index, which return echoes through the Bragg scatter mechanism (1,2,6; also described in the following section). Figure 8 shows the reflectivity fields associated with a cold front and a dry line, as well as the storms that initiated at the intersection of these boundaries. From Doppler velocity fields and observations of the cold front position at subsequent times, it was established that the cold air mass to the northwest of the front is colliding with the ambient air flowing from the SSW. The convergence along the boundary creates a line of persistent vertical motion that can lift scat-

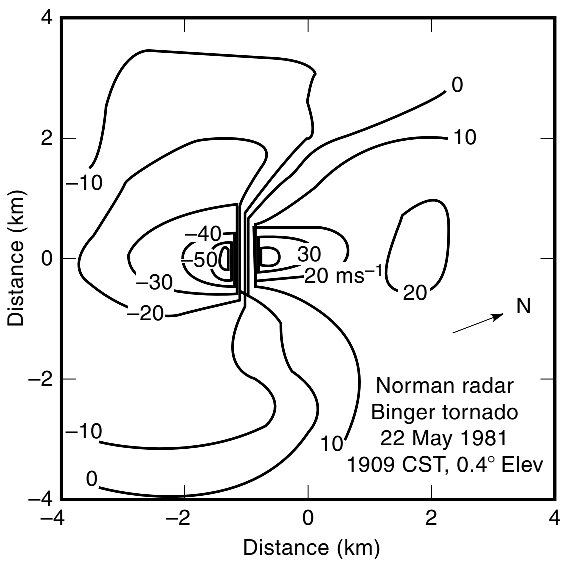

Figure 7. The isodops for the Binger, Oklahoma tornadic storm on 22 May 1981. The center of the mesocyclone is 70.8 km from the Norman Doppler radar at azimuth 284.4°; the data field has been rotated so that the radar is actually below the bottom of the figure.

tering particles, normally confined to the layers closer to the ground, making them visible as a reflectivity thin line. Thus, the reflectivity along the two boundaries could be due to these particles as well as to Bragg scatter. The intersection of cold fronts and dry lines is a favored location for the initiation of storms (seen to the northeast of the intersection). As the cold front propagates to the southeast, the intersection of it and the relatively stationary dry line progresses south-southwestward, and storms are initiated at this moving intersection point.

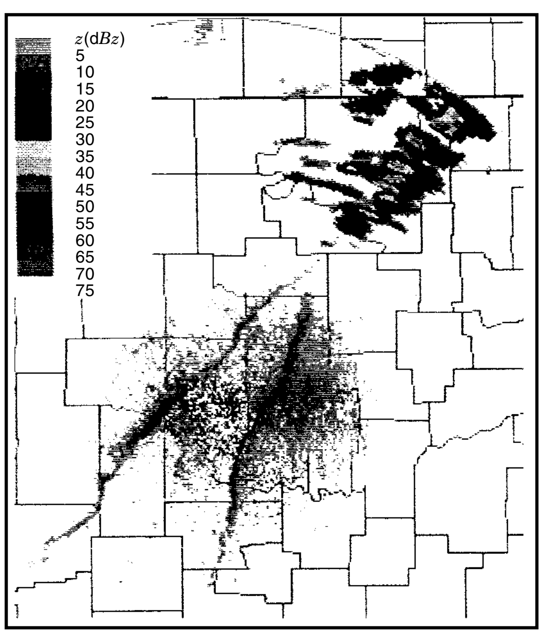

Figure 8. Intersecting reflectivity thin lines in central Oklahoma on 30 April 1991 at 2249 U. T. The thin line farthest west is along a NE-SW oriented cold front; the thin line immediately east is along a NNE-SSW oriented dry line. The reflectivity factor (dBZ) categories are indicated by the brightness bar. (Courtesy of Steve Smith, OSF/NWS.)

WIND AND TEMPERATURE PROFILES IN CLEAR AIR

In addition to particles acting as tracers of wind, irregularities of the atmosphere's refractive index can cause sufficient reflectivity to be detected by meteorological radars. Although irregularities have a spectrum of sizes, only those with scales of the order of half the radar wavelength provide echoes that coherently sum to produce a detectable signal (1). This scattering mechanism is called stochastic Bragg scatter because the half-wavelength irregularities are in a constant state of random motion due to turbulence, and thus the echo signal intensity fluctuates exactly like signals scattered from hydrometeors. The reflectivity η is related to the refractive index structure parameter C_n^2 that characterizes the itensity of the irregularities (1,2,7)

$$\eta = 0.38 C_n^2 \lambda^{-1/3} \qquad (13)$$

Mean values of C_n^2 range from about 10^{-14} m$^{-2/3}$ near sea level, to 10^{-17} m$^{-2/3}$ at 10 km above sea level.

Meteorological radars that primarily measure the vertical profile of the wind in all weather conditions and, in particular during fair weather, are called profilers. A wind profile is obtained by measuring the Doppler velocity vs range along beams in at least two directions (about 15 ° from the vertical) and along the vertical beam and by assuming that wind is uniform within the area encompassed by the beams. The vertical profile of the three components of wind can be calculated from these three radial velocity measurements along the range and the assumption of wind uniformity (7). A prototype network of these profilers has been constructed across the central United States to determine potential benefits for weather forecasts (8).

Temperature profiles are measured using a Radio-Acoustic Sounding System (RASS; 1,7). This instrument consists of a vertically pointed Doppler radar (for this application the wind profiling radar is usually time-shared) and a sonic transmitter that generates a vertical beam of acoustic vibrations, which produce a backscattering sinusoidal wave of refractive index propagating at the speed of sound. The echoes from the acoustic waves are strongest under Bragg scatter conditions (i.e., when the acoustic wavelength is one-half the radar wavelength). The backscatter intensity at various acoustic frequencies is used to identify those frequencies that produce the strongest signals.

Because the acoustic wave speed (and thus wavelength) is a function of temperature, this identification determines the acoustic velocity and hence the temperature. Allowance must be made for the vertical motion of air, which can be determined by analyzing the backscatter from turbulently mixed irregularities.

TRENDS AND FUTURE TECHNOLOGY

Networks of radars producing Doppler and reflectivity information in digital form have had a major impact on our capability to provide short-term warnings of impending weather hazards. Still, there are additional improvements that could enhance the information derived from meteorological radars significantly. Resolution of velocity and range ambiguities, faster coverage of the surveillance volume and better resolution, estimates of cross beam wind, and better measurements of precipitation type and amounts are some of the outstanding problems. Signal design techniques that encode transmitted pulses or stagger the PRT are candidates to mitigate the effects of ambiguities (1). Faster data acquisition can be achieved with multiple-beam phase-array radars, and better resolution can be obtained at the expense of a larger antenna. The cross beam wind component can be obtained using a bistatic dual-Doppler radar (i.e., combining the radial component of velocity measured by a Doppler weather radar with the Doppler shift measured at the distant receiver), or by incorporating the reflectivity and Doppler velocity data into the equations of motion and conservation. Vector wind fields in developing storms could be used in numerical weather prediction models to improve short-term forecasts. We anticipate an increase in application of millimeter wavelength Doppler radars to the study of nonprecipitating clouds (5). For better precipitation measurements, radar polarimetry offers the greatest promise (1,2). Polarimetry capitalizes on the fact that hydrometeors have shapes that are different from spherical and a preferential orientation. Therefore, differently shaped hydrometeors interact differently with electromagnetic waves of different polarization. To make such measurements, the radar should have the capability to transmit and receive orthogonally polarized waves, e.g., horizontal and vertical polarization. Both backscatter and propagation effects depend on polarization; measurements of these can be used to classify and quantify precipitation. Large drops are oblately shaped and scatter more strongly the horizontally polarized waves; they also cause larger phase shift of these waves along propagation paths. The differential phase method has several advantages for measurement of rainfall compared to the reflectivity method [Eq. (12)]. These include independence from receiver or transmitter calibrations errors, immunity to partial beam blockage and attenuation, lower sensitivity to variations in the distribution of raindrops, less bias from either ground clutter filtering or hail, and possibilities to make measurements in the presence of ground reflections not filtered by ground clutter cancelers. Polarimetric measurements have already proved the hail detection capability, but discrimination between rain, snow (wet, dry), and hail also seems quite possible. These areas of research and development could lead to improved short-term forecasting and warnings.

BIBLIOGRAPHY

1. R. J. Doviak and D. S. Zrnić, *Doppler Radar and Weather Observations,* 2nd ed., San Diego: Academic Press, 1993.
2. D. Atlas, *Radar in Meteorology,* Boston: Amer. Meteorol. Soc., 1990.
3. L. J. Battan, *Radar Observations of the Atmosphere,* Chicago: Univ. of Chicago Press, 1973.
4. R. Meneghini and T. Kozu, *Spaceborne Weather Radar,* Norwood, MA: Artech House, 1990.
5. *Proc. IEEE; Spec. Issue Remote Sens. Environ.,* **82** (12): 1994.
6. E. E. Gossard and R. G. Strauch, *Radar Observations of Clear Air and Clouds,* Amsterdam: Elsevier, 1983.
7. S. F. Clifford et al., Ground-based remote profiling in atmospheric studies: An overview, *Proc. IEEE,* **82** (3): 1994.
8. U.S. Department of Commerce, National Oceanic and Atmospheric Administration, *Wind profiler assessment report and recommendations for future use 1987–1994,* Prepared by the staffs of the National Weather Service and the Office of Oceanic and Atmospheric Research, Silver Spring, MD, 1994.

RICHARD J. DOVIAK
DUŠAN S. ZRNIĆ
National Severe Storms Laboratory
The University of Oklahoma

METER, PHASE. See PHASE METERS.
METERS. See OHMMETERS; POWER SYSTEM MEASUREMENT.
METERS, ELECTRICITY. See WATTHOUR METERS.
METERS, REVENUE. See WATTHOUR METERS.
METERS, VOLT-AMPERE. See VOLT-AMPERE METERS.
METHOD OF MOMENTS SOLUTION. See INTEGRAL EQUATIONS.
METHODS, OBJECT-ORIENTED. See BUSINESS DATA PROCESSING.
METHODS OF RELIABILITY ENGINEERING. See RELIABILITY THEORY.
METRIC CONVERSIONS. See DATA PRESENTATION.
METRICS, SOFTWARE. See SOFTWARE METRICS.